Geophysical Research Letters

RESEARCH LETTER
10.1029/2025GL116541

Increase in ENSO Frequency and Intensity Under 20th and 21st Century Warming: Insights From CMIP6 Large Ensembles

Arthur Coquereau[1], Florian Sévellec[1], Thierry Huck[1], and Alexey V. Fedorov[2]

[1]Laboratoire d'Océanographie Physique et Spatiale, University Brest CNRS IRD Ifremer, Brest, France, [2]Department of Earth & Planetary Sciences, Yale University, New Haven, CT, USA

Key Points:

- ENSO frequency and intensity increase in the 20th and 21st centuries in large ensembles and these changes scale with anthropogenic forcing
- The frequencies and intensity of both Eastern Pacific (EP) and Central Pacific variability increase
- The ENSO EP pattern-with its higher frequency-becomes more dominant in future projections, increasing ENSO frequency and intensity

Supporting Information:

Supporting Information may be found in the online version of this article.

Correspondence to:

A. Coquereau,
arthur.coquereau@univ-brest.fr

Citation:

Coquereau, A., Sévellec, F., Huck, T., & Fedorov, A. V. (2025). Increase in ENSO frequency and intensity under 20th and 21st century warming: Insights from CMIP6 large ensembles. *Geophysical Research Letters*, *52*, e2025GL116541. https://doi.org/10.1029/2025GL116541

Received 15 APR 2025
Accepted 2 NOV 2025

Author Contributions:

Conceptualization: Arthur Coquereau, Florian Sévellec, Alexey V. Fedorov
Formal analysis: Arthur Coquereau
Funding acquisition: Arthur Coquereau, Florian Sévellec
Investigation: Arthur Coquereau, Florian Sévellec, Thierry Huck, Alexey V. Fedorov
Methodology: Arthur Coquereau, Florian Sévellec, Thierry Huck, Alexey V. Fedorov
Project administration: Florian Sévellec
Supervision: Florian Sévellec, Thierry Huck, Alexey V. Fedorov
Visualization: Arthur Coquereau
Writing – original draft: Arthur Coquereau

Abstract Future changes in El Niño-Southern Oscillation (ENSO), the dominant mode of global climate variability, remain uncertain. Accordingly, large ensembles—which allow internally-generated variations to be averaged out—are essential for assessing the response of ENSO to external forcing. In this study, we analyze state-of-the-art large-ensemble simulations from CMIP6 climate models and show that, in most models, ENSO frequency increases under anthropogenic warming. Two factors drive this frequency increase. First, a shift toward the Eastern Pacific (EP) El Niño pattern—characterized by higher frequencies and greater amplitudes relative to the Central Pacific (CP) pattern. Second, an overall increase in the frequency of both EP and CP variability. These changes scale with the intensity of anthropogenic forcing. Most models also exhibit ENSO strengthening that begins in the 20th century and continues throughout the 21st century. Consequently, the observed intensification of ENSO during the second half of the 20th century could be of anthropogenic origin.

Plain Language Summary The El Niño-Southern Oscillation (ENSO) is a dominant mode of climate variability arising from ocean-atmosphere interactions in the equatorial Pacific. Because of its influence on sea surface temperature, precipitation, and winds, it has pronounced impacts on societies and ecosystems across the Pacific and beyond. Therefore, understanding how ENSO will change under anthropogenic global warming is a crucial research question. In this study, we analyze state-of-the-art climate models under several future anthropogenic emission scenarios to investigate these changes. We first examine shifts in ENSO frequency, focusing on changes in two main El Nino patterns—characterized by warm anomalies centered in the Eastern Pacific or Central Pacific, respectively. Our findings indicate that most models show an increasing ENSO frequency driven by two factors, often acting together: (a) a progressive dominance of the Eastern Pacific pattern—characterized by higher frequencies—over the Central Pacific pattern, and (b) an increase in the frequency of both Eastern and Central Pacific patterns. These changes appear to scale with the intensity of the anthropogenic forcing. Additionally, most models exhibit a gradual strengthening of ENSO throughout the 20th and 21st centuries. The combination of ENSO strengthening and frequency increase has major consequences for the tropical Pacific climate and ecosystems.

1. Introduction

Earth's climate is a complex system composed of various interconnected elements that naturally vary across a wide range of temporal and spatial scales (Baede et al., 2001; IPCC, 2021). In climate studies, this variability is often divided into two components: internally-generated and externally-driven variability (Baede et al., 2001; IPCC, 2021). Internal variability arises from interactions among scales and processes associated with the dynamics of the climate system itself (Deser & Phillips, 2023). Among its components, climate modes play a major role at the global scale (Cassou et al., 2021). Perhaps, the most important mode, El Niño-Southern Oscillation (ENSO), is driven by the tight coupling between the tropical ocean and atmosphere, which governs feedbacks and non-linear responses, leading to strong fluctuations in temperature, wind, and precipitation across the tropical Pacific, as well as in remote regions (e.g., Cai et al., 2021; Wang et al., 1999). In contrast, external or forced variability stems from external influences on the system, such as anthropogenic greenhouse gas emissions or volcanic eruptions (e.g., S. Hu & Fedorov, 2017; Möller et al., 2022).

In observations, internal and forced variability are intertwined within the time series of climate signals. In the context of anthropogenic climate change, disentangling these two components poses a major challenge for climate scientists. Traditionally, researchers have used time-filtering techniques or polynomial fits to extract the

Writing – review & editing:
Arthur Coquereau, Florian Sévellec, Thierry Huck, Alexey V. Fedorov

low-frequency signal assumed to reflect the anthropogenic forcing trend (e.g., Hawkins & Sutton, 2009; Lehner et al., 2020). Anomalies around this trend are then attributed to internal variability. However, this framework has multiple limitations. e.g., it requires either arbitrarily choosing a suitable mathematical function or defining a specific filtering time to separate internal variability from externally-forced variability. Since forced variability is typically associated with long-term trends, this framework would also tend to incorrectly attribute high frequency events like volcanic eruptions to internal variability (e.g., Parker et al., 1996). Conversely, internal variability can lead to longer-term variations, such as multidecadal oscillations (e.g., Ting et al., 2009; see Fedorov et al., 2020 for a review). Such low-frequency fluctuations can impact the trend and be incorrectly attributed to the forcing signal. These attribution errors can have a direct impact on the analysis of global warming and its effects on internal variability.

Recently, the ability to run ensemble climate simulations, thanks to advances in computing capacity, has led to substantial progress in the field (Deser et al., 2012, 2020; Maher et al., 2021). These ensemble simulations consist of sets of numerical experiments (known as ensemble members) from the same model, each covering the same time period and using identical external forcing. The only difference among these simulations lies in initial conditions, which allows exploring a range of possible system evolutions. By analyzing these simulations, it becomes possible to better extract the forced variability—defined as the mean signal across all members at a given time—from the internal variability, represented by the spread of members around this mean. This separation facilitates the analysis of human-induced changes in radiative forcing and their effect on internal variability (e.g., Maher et al., 2021).

In a previous study, we employed this large-ensemble framework to examine changes in the internal variability of surface temperature and precipitation at global scale (Coquereau et al., 2024). We analyzed state-of-the-art ensemble climate models from the 6th Phase of the Coupled Model Intercomparison Project (CMIP6, Eyring et al., 2016) over the historical period followed by different shared socioeconomic pathways (SSP) for the 21st century. Our findings demonstrated that internal variability is sensitive to external forcing, with significant changes observed in both temperature and precipitation variability in the equatorial Pacific. More specifically, we identified an increased frequency of internal variability in this region, which may be linked to a higher frequency and, to a lesser extent, intensity of ENSO.

In recent decades, numerous studies have examined how ENSO might respond to the observed and projected greenhouse gas emissions. Under increasing radiative forcing, many climate models generate a stronger ENSO sea surface temperature (SST) variability as well as the weakening of the mean east-west SST gradient (e.g., Cai et al., 2018, 2021; Fedorov & Philander, 2000, 2001; Ferrett & Collins, 2019; Fredriksen et al., 2020; Heede & Fedorov, 2023a; Maher et al., 2023). This future reduction in the zonal SST gradient aligns with an El Niño-like future mean warming of the eastern equatorial Pacific (Cai et al., 2021; Fu & Fedorov, 2023; Heede & Fedorov, 2021, 2023b; Maher et al., 2023).

Additionally, there are indications of greater variability and associated frequency in the Eastern Pacific (EP) El Niño events in the future, including extreme warm events, which may scale with the intensity of forcing (Cai et al., 2021, 2023; Fredriksen et al., 2020; Heede & Fedorov, 2023a; Vaittinada Ayar et al., 2023). Central Pacific (CP) events and La Niña events are also projected to increase in variability and frequency, although these changes may take longer to emerge compared to EP events (Cai et al., 2021, 2023; Geng et al., 2022; Vaittinada Ayar et al., 2023). This delayed response could be attributed to the stronger rainfall response associated with EP events, amplifying SST variability through atmospheric noise and potential nonlinear feedbacks (Cai et al., 2021; Geng et al., 2022; Heede & Fedorov, 2023a).

While these studies provide valuable and detailed analyses of ENSO future changes, they have primarily relied on single-member simulations (Fredriksen et al., 2020; Geng et al., 2022; Vaittinada Ayar et al., 2023) or small ensembles (Heede & Fedorov, 2023a). However, recent works (e.g., Cai et al., 2018; Maher et al., 2018) have demonstrated that 30 to 40 ensemble members are necessary to robustly separate forced trends from internal variability in ENSO. Furthermore, Lee et al. (2021) suggest that while 6 to 12 members are sufficient to robustly simulate the climatology and main teleconnections, analyzing ENSO characteristics and associated physical processes requires at least 50 ensemble members. Finally, another study shows that uncertainty in ensemble-mean and -variance decreases proportionally to the square root of ensemble size, reinforcing the value of large ensembles (Planton et al., 2024).

These and other recent studies have provided initial analyses of large ensembles, with detailed results that allow better separation of forced changes from internal variability (Cai et al., 2023; Maher et al., 2018, 2023). However, while these studies explored the future changes in specific events (e.g., strong El Niño or La Niña events), they have not examined changes in the overall frequency of ENSO, which is the main objective of the present work. Furthermore, theses studies typically focused on a single scenario, which limits the possibility of exploring how results may vary as a function of forcing intensity. This calls for a large-ensemble analysis that would specifically address changes in ENSO frequency and intensity both in the 20th and 21st centuries and their dependence on the magnitude of external forcing.

We also note that some studies, especially those using abrupt CO_2 quadrupling experiments, argue that ENSO may actually weaken with future warming (e.g., Callahan et al., 2021; Kohyama et al., 2018; Wengel et al., 2021). This contradiction might be associated with a nonlinear response of ENSO to changes in the mean state, as suggested by Geng et al. (2024) and Pontes et al. (2025), or with the unrealistically strong abrupt forcing applied. These differences also call for using large ensembles and a broad range of realistic climate scenarios to disentangle this complex response.

In this study, we address these challenges by using a collection of large-ensemble future climate simulations from CMIP6 to examine how ENSO frequency and intensity may respond to increasing anthropogenic forcing in several climate scenarios. In the next section, we describe the data and the methodology used in this work. Following this, we present our results in Section 3, which are then summarized and discussed in Section 4.

2. Material and Methods

2.1. CMIP6 Ensemble Simulations

The study is based on monthly Sea Surface Temperature (SST) data from CMIP6 ensemble models. Our analysis spans the historical period from 1850 to 2015 and includes four forcing scenarios for the 21st century: "Sustainability" (SSP1-2.6) with a low radiative forcing of 2.6 W m^{-2} by 2100, "Middle of the Road" (SSP2-4.5) with a radiative forcing of 4.5 W m^{-2}, "Regional rivalry" (SSP3-7.0) with a radiative forcing of 7.0 W m^{-2}, and "Fossil-fueled Development" (SSP5-8.5) with a high radiative forcing of 8.5 W m^{-2}.

Five ensemble models were available for all four forcing scenarios, each with at least 14 members. These models include MIROC6 (Tatebe et al., 2019, 50 members), ACCESS-ESM1-5 (Ziehn et al., 2020, 40 members), MPI-ESM1-2-LR (Olonscheck et al., 2023, 30 members), CanESM5 (Swart et al., 2019, 25 members), and GISS-E2-1-G (Kelley et al., 2020, 14 members). In addition, we examined a much larger ensemble, CESM2-LENS (Rodgers et al., 2021, 100 members), which allows for a more accurate separation between internal variability and the forced response. However, this ensemble is only available for the "Regional rivalry" (SSP3-7.0) scenario, and thus does not permit investigation of sensitivity to different forcings. Recent studies have demonstrated that the two CESM2-LENS sub-ensembles—distinguished by differing biomass burning emissions—exhibit distinct behaviors in Northern Hemisphere warming and sea ice loss (DeRepentigny et al., 2022; Fasullo et al., 2022). Nevertheless, our analysis reveals no significant differences in ENSO variability between these sub-ensembles. Consequently, they are treated as a single ensemble in this work. A summary of data is provided in Table S1 in Supporting Information S1 and the different physics used in GISS-E2-1-G are discussed in Text S1. To extract the long-term evolution of the climate state from the time series, a 30-year low-pass filter was applied.

A recent evaluation (Hou & Tang, 2022) shows that these models generally perform well in capturing ENSO characteristics including both the Eastern (EP) and Central Pacific (CP) patterns. ACCESS-ESM1-5 and CanESM5 show some limitations in accurately representing the EP and CP spatial structures, although their seasonal behavior and periodicity are well simulated. CESM2 has more difficulty reproducing the CP pattern but captures the EP pattern relatively well. Another comprehensive evaluation (Planton et al., 2021) confirms that the selected models rank among the best performers overall, accurately representing key ENSO processes, including the patterns, event duration, and diversity. At the same time, this assessment ranks MPI-ESM1-2-LR the lowest among the models considered in our study.

2.2. The Nino3.4 Index and Its Variability

The first analysis is based on the Nino3.4 SST index, defined as the mean monthly SST anomaly averaged over the 120–170°W and 5°S–5°N box, in the equatorial Pacific (Trenberth, 1997). The use of ensemble simulations allows us to calculate all anomalies across the ensemble rather than the time dimension, thereby limiting the statistical impacts of changes in the reference state (e.g., the impact of the warming trend). ENSO variability is then quantified as the variability among realizations (ensemble dimension) within a single model or across a collection of models (see Section 2.3). Ensemble statistics enable a more accurate separation of internal and forced variability, eliminating approximations related to detrending and avoiding reliance on the ergodic hypothesis—an assumption inherent in time-based statistics.

2.3. Multi-Model Mean

The computation of the multi-model mean values follows the bootstrapping methodology proposed in Coquereau et al. (2024). The approach involves extracting a sub-ensemble from each model by randomly selecting a fixed number of members (14 in this case). The five sub-ensembles (one per model) are then combined into a single multi-model ensemble consisting of $14 \times 5 = 70$ members. The analysis is conducted on this combined ensemble. This process is repeated multiple times ($N = 100$ iterations here), each time selecting different members randomly (with replacement). Sensitivity tests indicate no significant differences between using 100 and 1,000 resamplings. Finally, the results from these iterations are averaged to ensure robust conclusions and the associated 95% confidence interval is computed using the 2.5th and 97.5th percentile of the resamplings. CESM2-LENS is not included in the multi-model mean, as it is available only for one scenario (SSP3-7.0).

2.4. Separation of Frequencies

The period bands of ENSO variability are separated using filtering methodology applied on ensemble-variance time series, as described in Text S2. This filtering approach was chosen because it allows for an investigation of the temporal evolution of the variance spectrum. Based on an initial analysis of the spectra, we chose four period bands (<1, 1–3, 3–5, and >5 years), in order to agglomerate bands with consistent behavior and facilitate presentation and interpretation of the results.

2.5. Separation of Eastern Pacific and Central Pacific Patterns

To investigate the roles of EP and CP patterns, we use a Principal Component Analysis (PCA) of SST anomalies in a larger equatorial domain from 140°E to 80°W and 15°S to 15°N (Cai et al., 2018; Dommenget et al., 2013; Takahashi et al., 2011). This allows the CP and EP indices to be derived from a combination of the first two modes of PCA. A comprehensive description of the methodology is provided in Text S3 in Supporting Information S1.

Recent studies have utilized large ensembles to compute distinct EOFs for individual time-step snapshots (e.g., Haszpra et al., 2020; O'Brien & Deser, 2023), enabling analysis of the temporal evolution of the spatial structure of climate modes. While these methods are highly informative, they assume that variance consistently projects onto the leading modes of the decomposition, typically the first two EOFs. However, in theory, the distribution of variance explained among the modes may shift when EOFs are computed over different time steps, as there is no guarantee that variance will partition identically across modes for varying input data sets.

In this study, we do not employ these snapshot-EOF methods. Instead, we compute a single EOF decomposition per model (with spatial patterns corresponding to sets of features), across all time steps, ensemble members and scenarios (corresponding to different samples of the features). This approach allows us to consistently track changes in the identified mode over time and under the influence of anthropogenic forcing. Additionally, ensemble members are considered as out-of-phase realizations of the same climate system—what is observed in one member should, in principle, be observable in another at a different time step. Therefore, there is no justification for computing separate EOFs for the different members, provided that the decomposition is performed over a sufficiently long time period to accurately capture the variability.

While this method does not address the non-stationarity of climate modes—a topic already explored in the literature (e.g., Haszpra et al., 2020; O'Brien & Deser, 2023)—its strength lies in robustly tracking changes in identified spatial patterns. This capability fills a gap in the literature on ensemble-based ENSO analysis.

10.1029/2025GL116541

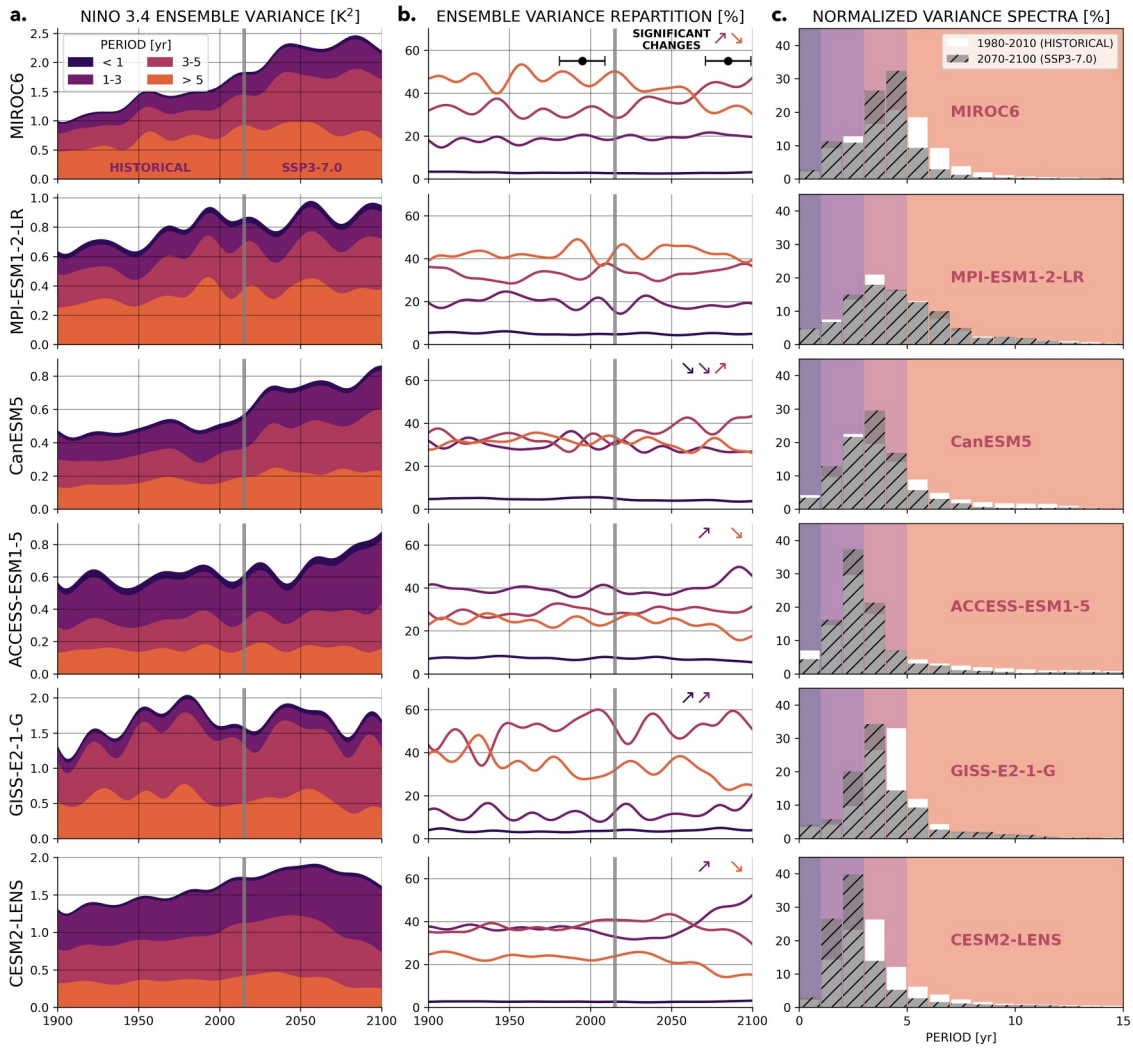

Figure 1. Evolution of Nino3.4 SST variance and associated frequencies over time in large ensembles of different climate models. (a) Temporal evolution of variance (in K^2) for different period bands (<1, 1–3, 3–5, and >5 years). Each row shows changes during the historical period and under the SSP3-7.0 scenario for the projection period for a given model. (b) Relative variance contribution of each period band over time (colors identical to panel a). Arrows in the top right corner indicate whether a frequency band (represented by its corresponding color) has significantly increased or decreased from 1980 to 2010 to 2070–2100 (horizontal segments), based on a 95% confidence interval (see Section 2.3). (c) Normalized variance spectra of the Nino3.4 index for the 1980–2010 historical period (white) and the 2070–2100 projection period (gray hatched). Background colors indicate the period bands shown in panels (a) The vertical gray lines correspond to the year 2015 and separate the historical period from the projections. A 30-year low-pass filter was applied to extract the long-term evolution of the climate state from the time series.

3. Results

3.1. Changes in ENSO SST Variability and Frequency

We begin our investigation of changes in ENSO variability by employing the widely used Nino3.4 index, based on spatially-averaged SST anomalies in the equatorial Pacific (see Section 2.2). First, we estimate changes in ENSO variance for the different models under the forcing scenario common to all models: SSP3-7.0. All six models analyzed exhibit an overall increase of the total ENSO variability under this scenario (Figure 1a) up to the middle of the 21st century. Then, in the second half of the 21st century, following the initial increase of variance, one model stabilizes (GISS-E2-1-G), one model indicates a decline (CESM2-LENS), and the remaining four other models show a continuing increase. We emphasize that the increase in ENSO variability across all six models begins in the first half of the 20th century and continues throughout the historical simulations.

Going beyond these changes in variance intensity, we next focus on the changes in ENSO frequency. Here, we separate the total variance into four period bands: shorter than 1 year, between 1 and 3 years, between 3 and

5 years, and longer than 5 years (see Section 2.4). All models exhibit a mean decline during the 21st century in the relative variance associated with periods longer than 5 years (orange line, Figure 1b), which is significant at the 95% confidence level in 3 out of 6 models. Depending on the model, this decrease is either compensated by a relative increase in the 1–3 years period band (CESM2-LENS), a relative increase of the 3–5 years band (MPI-ESM1-2-LR and CanESM5), or both (MIROC6, ACCESS-ESM1-5 and GISS-E2-1-G). In CESM2-LENS, the increase in 1–3 years band also compensates for a decrease in the 3–5 years band. These results, therefore, indicate an overall tendency for ENSO variability to shift toward higher frequencies in the 21st century.

Overall, nearly all models exhibit significant changes in the variance spectrum between the periods 1980–2010 and 2070–2100 (Figure 1c), consistent with our previous findings from the time series analysis (Figure 1b). These 30-year periods, which are standard for climate statistics (e.g., Arguez & Vose, 2011), were selected to assess projected changes by the end of the 21st century under various forcing scenarios relative to present-day conditions. For MPI-ESM1-2-LR, changes in the normalized variance spectrum are, however, less pronounced and changes in the temporal evolution across different frequency bands appear to be not significant.

To summarize the above results, we have also computed multi-model means, using the bootstrap methodology detailed in Section 2.3. It allows us to analyze the link between these changes in ENSO frequency and the magnitude of anthropogenic forcing. The multi-model mean evolution of the variance shows a decline in lower frequencies (>5 years) and an increase in higher frequencies (1–3 years and 3–5 years) (Figure 2a), which are robust with a 95% confidence level (Table S2 in Supporting Information S1). This trend toward an increase in ENSO frequency throughout the 21st century is also confirmed by the multi-model variance spectra (Figure 2b). That is, the spectrum shifts toward higher frequencies from the period 1980–2010 to 2070–2100. From both diagnostics, this shift appears to be directly linked to the magnitude of the forcing, especially for the 1–3 and >5 years period bands. This is confirmed by the 2070–2100 average for each scenario (Table S2 in Supporting Information S1).

Although these results indicate significant and robust changes, the slightly different behavior exhibited by one of the models (MPI-ESM1-2-LR) remains to be reconciled with the results of other modes. To address this gap in understanding, we delve deeper into the analysis of ENSO by separating its variability into two main patterns: Eastern Pacific (EP) and Central Pacific (CP).

3.2. Transition From Central to Eastern-Pacific Dominated ENSO Variability

The separation of EP and CP patterns requires leaving aside the Nino3.4 index and using another methodology based on Principal Components Analysis (PCA) described in Section 2.5. Using a rotation of the two first modes of variability (i.e., EOF1 and EOF2, Figure S2 in Supporting Information S1), we can obtain the two patterns associated with intensified variability in the eastern or central equatorial Pacific (Figure S3 in Supporting Information S1). The different models present a relatively good agreement between each other in terms of shape and intensity of patterns. The patterns are consistent with those described from observations (e.g., Kao & Yu, 2009), with CP intensified between 110 and 160°W, EP peaking between 90 and 140°W (Figure S3 in Supporting Information S1), and both patterns exhibiting a variance of approximately 1 K^2 (Figure 3).

All models exhibit a substantial increase in the absolute variance of the EP index over time, which appears to scale, to some extent, with the intensity of the forcing scenario (Figures 3a and 3c). In MIROC6 and CESM2-LENS, the EP variance doubles (+109% and +97%) from 1900 to 1930 to 2070-2100 under SSP3-7.0, passing from 0.59 to 1.23 K^2 and from 0.72 to 1.41 K^2. The four other models also present important increases spanning from +16% to +57%. Regarding the CP pattern, while CanESM5 shows a substantial increase over time proportional to the forcing strength, the other models show either increases followed by decreases (MIROC6, ACCESS-ESM1-5, GISS-E2-2-G and CESM2-LENS) or unclear trends (MPI-ESM1-2-LR). These changes in the EP and CP patterns induce an increase in the EP pattern's relative contribution to the total variance compared to CP and thus an increase of EP-to-CP variance ratio. Except for CanESM5, all models exhibit a transition over time from being CP-dominated to being dominated by the EP pattern.

The results above need to be put in the perspective of the dominant variability bands of the CP and EP patterns. Indeed, for all models investigated, the CP pattern corresponds to lower frequencies than the EP pattern. CP is dominated by the >5 years period band (Figure 3b), while EP is dominated by 1–3 years period band in 4 models, and presents no dominant frequency from 1 to 3 to >5 years in the two other models (Figure 3c). This seems to be

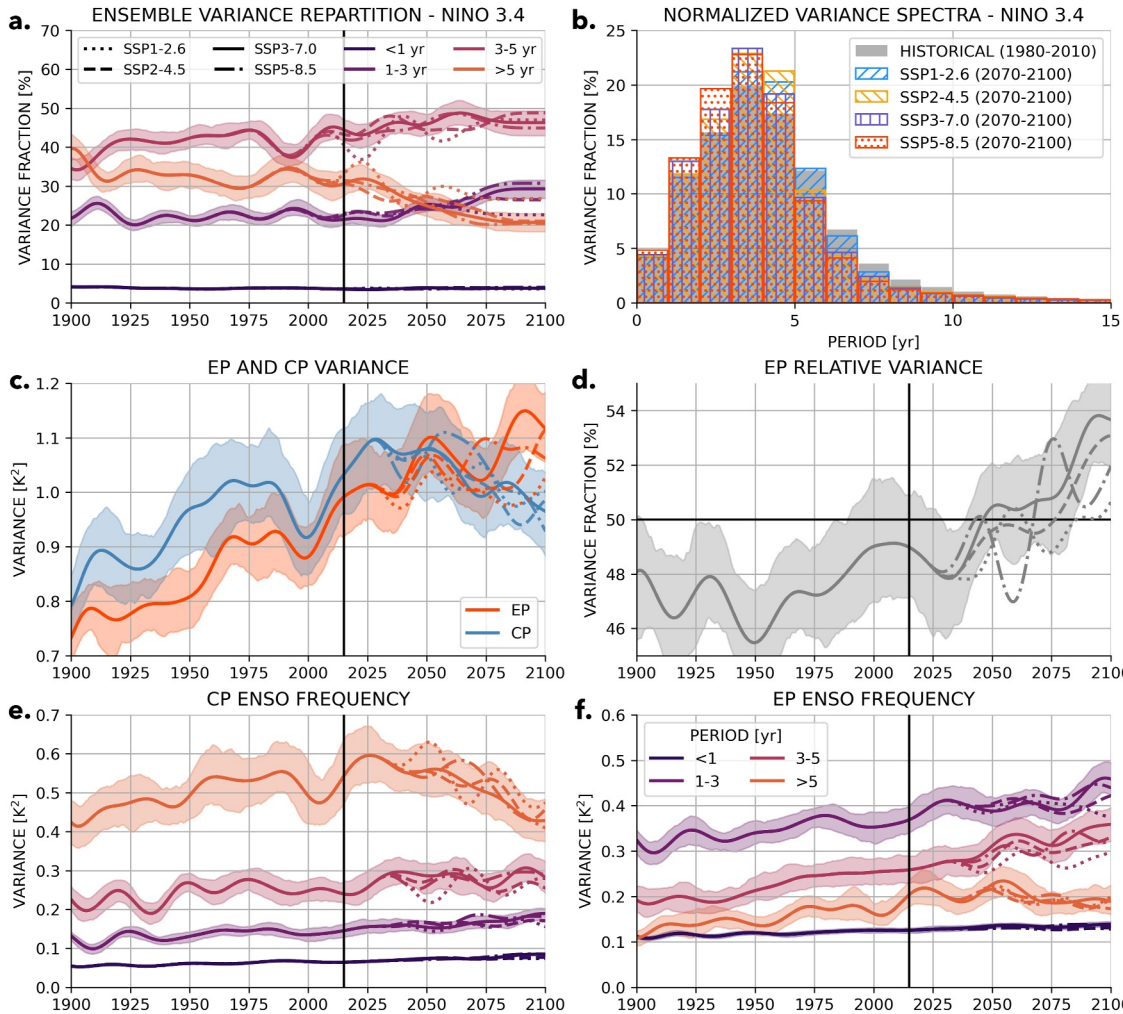

Figure 2. Evolution of multi-model mean variance and associated frequencies. (a) Temporal evolution of relative variance of the Nino3.4 SST index for different period bands (<1 year, 1–3 years, 3–5 years and >5 years) and under different scenarios: SSP1-2.6 (dotted line), SSP2-4.5 (dashed line), SSP3-7.0 (solid line), and SSP5-8.5 (dash-dotted line). (b) Normalized variance spectra of the Nino3.4 SST index for the 1980-2010 historical period (in gray) and the 2070-2100 projection period under different scenarios: SSP1-2.6 (blue), SSP2-4.5 (orange), SSP3-7.0 (purple), and SSP5-8.5 (red). (c) Variance associated with the Eastern Pacific (red) and Central Pacific (blue) patterns over the historical period and under different forcing scenarios. (d) EP relative variance, under different scenarios. (e) CP and (f) EP variability associated with different period bands, and under different forcing scenarios. For panel c–f, after the year 2015, line styles represent different scenarios as defined in panel (a) Shading represents a 95% confidence interval associated with the bootstrapping for historical and SSP3-7.0 time series (method detailed in Section 2.3). Mean values and statistical tests are given in Table S2 in Supporting Information S1. The vertical black lines correspond to the year 2015, which separates the historical period from future scenarios. A 30-year low-pass filter was applied to extract the long-term evolution of the climate state from the time series.

consistent with the low-frequency decadal variability of CP ENSO observed in the literature, which has an impact on its spectrum (e.g., Furtado et al., 2012). Hence, the fact that ENSO variability becomes progressively dominated by EP pattern, whose variance is in general of higher frequency than that of the CP pattern in CMIP6 models, is critical for the increasing ENSO frequency noted in Section 3.1.

The second factor lies in the frequency change of each pattern. Indeed, all models reveal a decrease of the variance associated with the >5 years band for the CP pattern (Figure 3b). This decrease is partially compensated by increasing CP variance at higher frequencies in many models, either both in the 1–3 and 3–5 years period bands (MIROC6, CanESM5 and ACCESS-ESM1-5), or in the 1–3 years band only with a decrease in the 3–5 years band (GISS-E2-2-G and CESM2-LENS). In addition, changes in frequency are also observed for the EP patterns (Figure 3c). After an initial increase, the low frequencies decrease in four models both in terms of relative and absolute contributions (MIROC6, ACCESS-ESM1-5, GISS-E2-2-G and CESM2-LENS). The variance in the 1–3 years band increases across all models, except for MPI-ESM1-2-LR, where it remains stable. Similarly, the

10.1029/2025GL116541

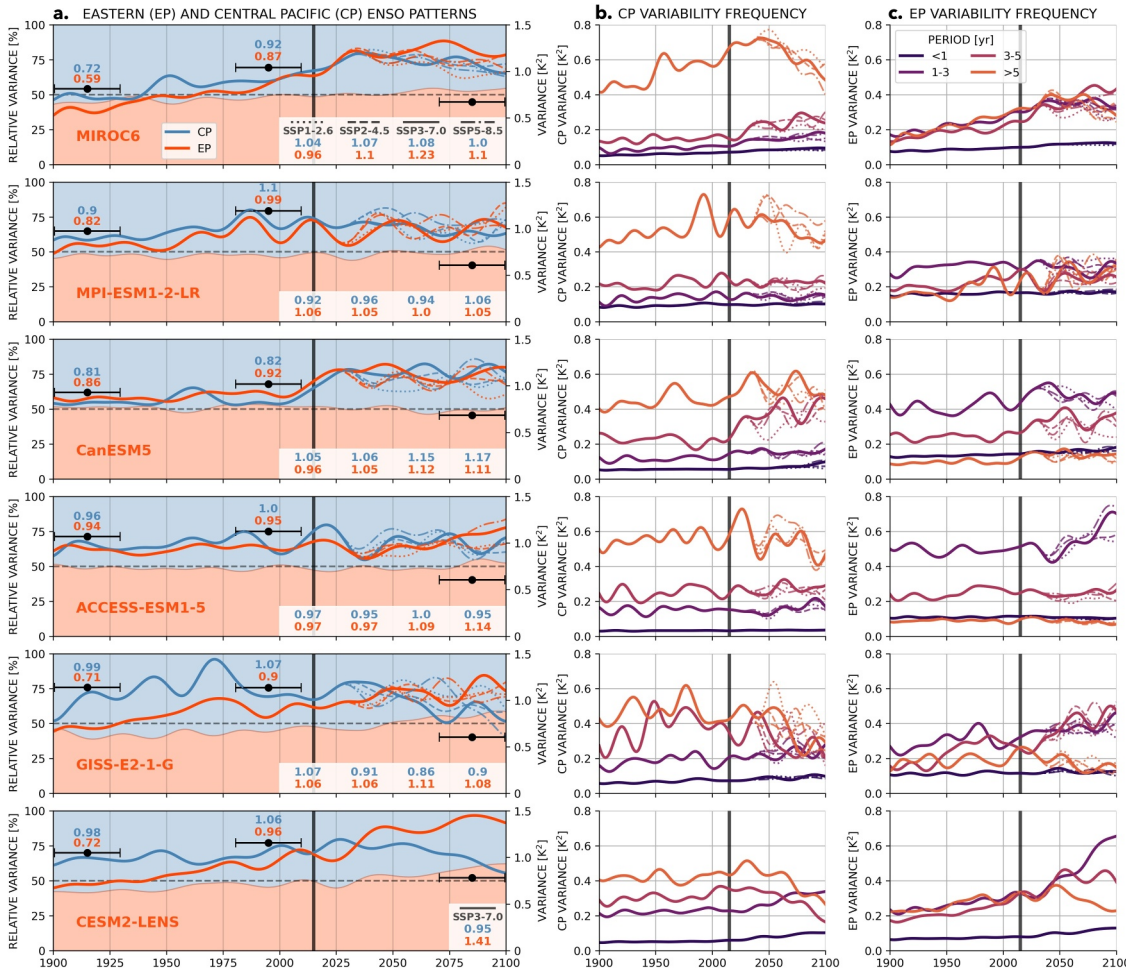

Figure 3. Evolution of ENSO variability associated with Eastern Pacific (EP) and Central Pacific (CP) patterns. (a) Background colors represent the relative variance contribution of EP (red) and CP (blue) during the historical period and during the 21st century under the SSP3-7.0 scenario (black horizontal dashed lines show the 50% value). Lines represent the evolution of absolute variance of EP (red) and CP (blue) patterns for the historical period and different scenarios: SSP1-2.6 (dotted line), SSP2-4.5 (dashed line), SSP3-7.0 (solid line), and SSP5-8.5 (dash-dotted line). Mean variance values are displayed in the figure for three 30-year periods (1900–1930, 1980–2010, and 2070–2100) highlighted by horizontal black intervals (bottom-right white panel, shown for the three scenarios). These values can be used as a proxy for tracking changes in the dominant pattern over time. Evolution of (b) CP and (c) EP variability in the four period bands (<1 year, 1–3 years, 3–5 years, and >5 years) for the different forcing scenarios. For panels b and c, colors represent various period bands and are defined in panel (c) After 2015, line styles represent various scenarios and are defined in panel (a) Each row represents a different model. The vertical black lines correspond to year 2015 and separate the historical period from the scenario. A 30-year low-pass filter was applied to extract the long-term evolution of the climate state from the time series.

variance in the 3–5 years band increases in all models, except for ACCESS-ESM1-5, where it also remains stable. Finally, except for ACCESS-ESM1-5, all models exhibit an increase in intra-annual/seasonal variability (<1 year band) of the EP and CP patterns.

Considering these two mechanisms, we find that four models present both an increase in EP-to-CP variance ratio and an increasing frequency of the EP and CP patterns (MIROC6, ACCESS-ESM1-5, GISS-E2-2-G and CESM2-LENS). One model (CanESM5) shows only an increasing frequency in variance associated with the EP and CP patterns, and one model (MPI-ESM1-2-LR) shows a slight increase in the EP-to-CP variance ratio but compensated by a weakly decreasing frequency of both EP and CP variance.

Overall, the observed changes appear to scale with the forcing intensity, at least for the five models available for three different scenarios. 4/5 models reveal stronger increase of EP-to-CP ratio under SSP3-7.0 and SSP5-8.5 than under SSP1-2.6, 4/5 models reveal stronger increase of EP variance under SSP3-7.0 and SSP5-8.5 than under SSP1-2.6, and 3/5 show a stronger decrease in CP variance for SSP5-8.5 than SSP1-2.6 (Figure 3a). Considering changes in variance frequency for the EP and CP patterns, in general, the SSP5-8.5 presents the most extreme

change as compared to the other scenarios (dash-dotted line in Figures 3b and 3c). However, under the two strongest forcings (SSP3-7.0 and SSP5-8.5), the ENSO response does not always scale consistently with scenario intensity. Moreover, given the variability in the time series across the models, the link between changes and the forcing intensity requires further investigation.

To assess this link more robustly and draw a final, summarized picture of EP and CP variability changes, we have computed a multi-model mean based on the five models available for the four scenarios (Figures 2c–2f). The increase in EP variability, while CP variability is more or less stable, is logically responsible for an increasing EP variance contribution (Figures 2c and 2d), robust at the 95% confidence level (Table S2 in Supporting Information S1). This EP-to-CP ratio change appears to scale with forcing scenario intensity, although differences between the two strongest scenarios are not fully evident (Table S2 in Supporting Information S1). In addition, we detected an increase in the frequency of both the EP and CP patterns driven by a decline of the >5 years period band (robust for CP, Table S2 in Supporting Information S1) and an increase at higher frequencies (Figures 2e and 2f), robust for both patterns (Table S2 in Supporting Information S1). While SSP5-8.5 presents larger frequency changes than SSP1-2.6, it is less clear how the intermediate scenarios (SSP2-4.5 and SSP3-7.0) compare in term of magnitude of changes. Therefore, although we hypothesized a link between EP and CP frequency increase and the forcing intensity, the spread of changes under different scenarios is not sufficiently robust to demonstrate this link.

4. Conclusions and Discussion

In this study, we examined changes in ENSO sea surface temperature variability under global warming, using a range of forcing scenarios and CMIP6 large ensembles to ensure robust statistics and conclusions. Our findings indicate that most models considered exhibit an increasing frequency of Nino3.4 index variability from 1900 to 2100, which appears to scale with the magnitude of the external forcing. The frequency shift becomes particularly pronounced after the year 2050, and the timing of this change represents an interesting direction for future research. We also see a gradual increase in ENSO frequency already during the 20th century, evident in the multi-model mean (Figure 2a). Furthermore, most models exhibit an overall strengthening of ENSO throughout the 20th and the 21st centuries as well (Figure 1a).

The simulated increase in both the intensity and frequency of ENSO throughout the 20th century, as evident in the large ensembles, appears to resolve a long-standing question in climate science and suggests a potential anthropogenic origin for the ENSO intensification observed during the latter half of the 20th century, which culminated in the strongest ENSO activity on record in the 1980s and 1990s (e.g., Li et al., 2013).

Differences between the EP and CP ENSO patterns and their response to warming shed light on some of the projected changes. The EP pattern is typically associated with higher-frequency variability, and more intense El Niño events, whereas the CP pattern is associated with stronger La Niña but weaker El Niño events and lower frequency (Cai et al., 2021). In our study, we show that the overall increase in ENSO frequency is driven by two distinct factors. The first factor is an increase in the EP variance contribution to ENSO (and EP-to-CP ratio), as also described in the literature from observations (Cai et al., 2021) and climate simulations (Cai et al., 2021; Fredriksen et al., 2020; Geng et al., 2022; Heede & Fedorov, 2023a; Vaittinada Ayar et al., 2023). This drives a direct increase in ENSO frequency, since EP variability is characterized by a higher frequency.

The second driver is an increase in the frequencies of both EP and CP components of ENSO variability. It is driven by a decline in variability at timescales longer than 5 years and an increase in shorter-period fluctuations, particularly within the 1–5 years range. These two drivers are often combined, as it is observed in 4 out of 6 studied models. Additionally, one model shows an ENSO frequency increase driven solely by higher EP and CP variance frequency. Conversely, one model does not exhibit a strong frequency increase in its spectrum, due to the compensatory effects of the EP-to-CP ratio increase and a decline in the frequency of both EP and CP variability. In this analysis, we investigate the EP and CP patterns computed from the entire time series and track their temporal evolution. Given the profound changes affecting the system, several recent articles have also examined the evolution of these spatial patterns over time (e.g., Haszpra et al., 2020; O'Brien & Deser, 2023).

Differences between the EP and CP variabilities also explain the overall strengthening of ENSO observed in four models by the end of the 21st century, while the two others stabilize or weaken (GISS-E2-1-G and CESM2-

LENS). This peculiar behavior coincides with a substantial decline in CP ENSO variance in these two models, which could be a potential explanation for their trends.

Physically, the strengthening of the EP-to-CP ratio, partially responsible for the increase in frequency, is consistent with enhanced future mean warming in the eastern equatorial Pacific relative to the west, a pattern simulated by climate models and supported by recent studies (Cai et al., 2023; Fu & Fedorov, 2023; Geng et al., 2022; Heede & Fedorov, 2021, 2023a; Maher et al., 2023). This mean warming allows stronger western Pacific warm excursions to the east, leading to larger eastward shifts in atmospheric deep convection, which strengthens the positive Bjerknes feedback and in turn enhances EP SST variability. In addition, the increased frequency of EP and CP patterns individually may be linked to changes in the zonal SST gradient, which can be driven by external forcings but also modulated by remote internal climate oscillations, such as the Atlantic Multidecadal Oscillation (Gan et al., 2023) or changes in the Indian Ocean (Ferster et al., 2023), for a review see Fedorov et al. (2020) or A. Hu et al. (2025). A recent study also suggests that the displacement of the convergence zone toward the equator could be associated with ENSO higher frequencies, related to the annual cycle (Pontes et al., 2025).

Our results indicate the possible relationship between observed changes and the intensity of anthropogenic forcing, especially visible using multi-model means (Figure 2), or 30-year time averages (Figure 3a and Table S2 in Supporting Information S1). The relationship is supported by the weakest and strongest scenarios investigated, since SSP5-8.5 presents almost always stronger changes than SSP1-2.6. However, for other analyses such as changes in EP and CP frequency and for the intermediate scenarios, the relationship is less clear because of the remaining multidecadal variability, even after ensemble averaging.

The increasing role of EP variability is particularly concerning given that this pattern is generally associated with more extreme events (Heede & Fedorov, 2023a), which have stronger impacts on societies and ecosystems in the regions surrounding the Pacific (Dewitte et al., 2012; Pizarro et al., 2002).

A caveat of the results presented here is the limited collection of models studied, due to the relatively small number of large-ensemble climate simulations available. Additionally, one of the models (MPI-ESM1-2-LR) does not show such a clear change in ENSO frequency under global warming. However, since this model appears to be less accurate at simulating ENSO dynamics (Planton et al., 2021), this result may carry less weight in the overall analysis. Recent studies by Chung et al. (2024) and Stuivenvolt-Allen et al. (2025), based on more comprehensive collections of models but with much fewer ensemble members, report contrasting results regarding changes in ENSO frequency, with outcomes dependent on the models considered. Nevertheless, more than half of the models in Stuivenvolt-Allen et al. (2025) exhibit an increase in frequency, and it is challenging to distinguish the forced response from internal variability when using small ensembles (Cai et al., 2018). Critically, in our study, the multi-model mean clearly shows an increase in both the frequency and intensity of ENSO throughout the 20th and 21st centuries.

Another recent analysis based on large-ensemble models supports the future increase in EP event frequency, while findings are more mixed regarding changes in EP amplitude and CP frequency (Maher et al., 2022). The method used to separate EP and CP patterns is also subject to debate, as alternative approaches might yield different results (Abdelkader Di Carlo et al., 2023). However, it is important to emphasize that in the present study, our goal is not to define these patterns uniquely, but rather to examine how two dominant modes evolve over time and under different emission pathways. It has also been shown that CMIP6 models exhibit some limitations in reproducing observed historical trends in the tropical Pacific–for example, the cooling trends of the past several decades in the eastern Pacific (Heede & Fedorov, 2023b; Wills et al., 2022). Further progress in ENSO modeling is therefore needed to increase confidence in the projections provided by climate models.

Conflict of Interest

The authors declare no conflicts of interest relevant to this study.

Data Availability Statement

The CMIP6 ensemble models analyzed in this study are MIROC6 (Tatebe et al., 2019), ACCESS-ESM1-5 (Ziehn et al., 2020), MPI-ESM1-2-LR (Olonscheck et al., 2023), CanESM5 (Swart et al., 2019), and GISS-E2-1-G

(Kelley et al., 2020). The data can be downloaded from the various Earth System Grid Federation (ESGF) nodes. The 100 members from CESM2-LENS (Rodgers et al., 2021) can be downloaded from the NSF NCAR Climate Data Gateway (https://www.earthsystemgrid.org).

Acknowledgments
This work was supported by ISblue project, Interdisciplinary graduate school for the blue planet (ANR-17-EURE-0015) and co-funded by a Grant from the French government under the program "Investissements d'Avenir" embedded in France 2030. This work was also supported by the ARVOR project funded through the French CNRS/INSU/LEFE program. AVF acknowledges support from NOAA (NA20OAR4310377) and the US Department of Energy (DE-SC0023134), and from the ARCHANGE project (ANR-18-MPGA-0001, France).

References

Abdelkader Di Carlo, I., Braconnot, P., Carré, M., Elliot, M., & Marti, O. (2023). Different methods in assessing el Niño flavors lead to opposite results. *Geophysical Research Letters*, *50*(15), e2023GL104558. https://doi.org/10.1029/2023GL104558

Arguez, A., & Vose, R. S. (2011). The definition of the standard wmo climate normal: The key to deriving alternative climate normals. *Bulletin of the American Meteorological Society*, *92*(6), 699–704. https://doi.org/10.1175/2010bams2955.1

Baede, A. P. M., Ahlonsou, E., Ding, Y., & Schimel, D. S. (2001). The climate system: An overview. In *Climate change 2001: Impacts, adaptation and vulnerability* (pp. 87–98). Cambridge University Press.

Cai, W., Ng, B., Geng, T., Jia, F., Wu, L., Wang, G., et al. (2023). Anthropogenic impacts on twentieth-century ENSO variability changes. *Nature Reviews Earth and Environment*, *4*(6), 407–418. https://doi.org/10.1038/s43017-023-00427-8

Cai, W., Santoso, A., Collins, M., Dewitte, B., Karamperidou, C., Kug, J. S., et al. (2021). Changing El Niño-Southern Oscillation in a warming climate. *Nature Reviews Earth and Environment*, *2*(9), 628–644. https://doi.org/10.1038/s43017-021-00199-z

Cai, W., Wang, G., Dewitte, B., Wu, L., Santoso, A., Takahashi, K., et al. (2018). Increased variability of eastern Pacific El Niño under greenhouse warming. *Nature*, *564*(7735), 201–206. https://doi.org/10.1038/s41586-018-0776-9

Callahan, C. W., Chen, C., Rugenstein, M., Bloch-Johnson, J., Yang, S., & Moyer, E. J. (2021). Robust decrease in El Niño/Southern Oscillation amplitude under long-term warming. *Nature Climate Change*, *11*(9), 752–757. https://doi.org/10.1038/s41558-021-01099-2

Cassou, C., Cherchi, A., & Kosaka, Y. (2021). Annex IV: Modes of variability. In V. Masson-Delmotte, P. Zhai, A. Pirani, S. L. Connors, C. Péan, S. Berger, et al. (Eds.), *Climate change 2021: The physical science basis. contribution of working group i to the sixth assessment report of the intergovernmental panel on climate change* (pp. 2153–2192). Cambridge University Press. https://doi.org/10.1017/9781009157896.018

Chung, C. T. Y., Power, S. B., Boschat, G., Gillett, Z. E., & Narsey, S. (2024). Projected changes to characteristics of el niño-southern oscillation, indian ocean dipole, and southern annular mode events in the cmip6 models. *Earth's Future*, *12*(11), e2024EF005166. https://doi.org/10.1029/2024EF005166

Coquereau, A., Sévellec, F., Huck, T., Hirschi, J. J.-M., & Hochet, A. (2024). Anthropogenic changes in interannual-to-decadal climate variability in cmip6 multiensemble simulations. *Journal of Climate*, *37*(14), 3723–3739. https://doi.org/10.1175/JCLI-D-23-0606.1

DeRepentigny, P., Jahn, A., Holland, M. M., Kay, J. E., Fasullo, J., Lamarque, J.-F., et al. (2022). Enhanced simulated early 21st century arctic sea ice loss due to cmip6 biomass burning emissions. *Science Advances*, *8*(30), eabo2405. https://doi.org/10.1126/sciadv.abo2405

Deser, C., Lehner, F., Rodgers, K. B., Ault, T., Delworth, T. L., DiNezio, P. N., et al. (2020). Insights from Earth system model initial-condition large ensembles and future prospects. *Nature Climate Change*, *10*(4), 277–286. https://doi.org/10.1038/s41558-020-0731-2

Deser, C., Phillips, A., Bourdette, V., & Teng, H. (2012). Uncertainty in climate change projections: The role of internal variability. *Climate Dynamics*, *38*(3–4), 527–546. https://doi.org/10.1007/s00382-010-0977-x

Deser, C., & Phillips, A. S. (2023). A range of outcomes: The combined effects of internal variability and anthropogenic forcing on regional climate trends over Europe. *Nonlinear Processes in Geophysics*, *30*(1), 63–84. https://doi.org/10.5194/npg-30-63-2023

Dewitte, B., Vazquez-Cuervo, J., Goubanova, K., Illig, S., Takahashi, K., Cambon, G., et al. (2012). Change in El Niño flavours over 1958-2008: Implications for the long-term trend of the upwelling off Peru. *Deep Sea Research Part II: Topical Studies in Oceanography*, *77–80*, 143–156. https://doi.org/10.1016/j.dsr2.2012.04.011

Dommenget, D., Bayr, T., & Frauen, C. (2013). Analysis of the non-linearity in the pattern and time evolution of El Niño Southern Oscillation. *Climate Dynamics*, *40*(11–12), 2825–2847. https://doi.org/10.1007/s00382-012-1475-0

Eyring, V., Bony, S., Meehl, G. A., Senior, C. A., Stevens, B., Stouffer, R. J., & Taylor, K. E. (2016). Overview of the Coupled Model intercomparison project phase 6 (CMIP6) experimental design and organization. *Geoscientific Model Development*, *9*(5), 1937–1958. https://doi.org/10.5194/gmd-9-1937-2016

Fasullo, J. T., Lamarque, J.-F., Hannay, C., Rosenbloom, N., Tilmes, S., DeRepentigny, P., et al. (2022). Spurious late historical-era warming in cesm2 driven by prescribed biomass burning emissions. *Geophysical Research Letters*, *49*(2), e2021GL097420. https://doi.org/10.1029/2021GL097420

Fedorov, A. V., Hu, S., Wittenberg, A. T., Levine, A. F. Z., & Deser, C. (2020). Enso low-frequency modulation and mean state interactions. In *El niño southern oscillation in a changing climate* (pp. 173–198). American Geophysical Union (AGU). https://doi.org/10.1002/9781119548164.ch8

Fedorov, A. V., & Philander, S. G. (2000). Is El niño changing? *Science*, *288*(5473), 1997–2002. https://doi.org/10.1126/science.288.5473.1997

Fedorov, A. V., & Philander, S. G. (2001). A stability analysis of tropical ocean-atmosphere interactions: Bridging measurements and theory for El niño. *Journal of Climate*, *14*, 3086–3101. https://doi.org/10.1175/1520-0442(2001)014⟨3086:ASAOTO⟩2.0.CO;2

Ferrett, S., & Collins, M. (2019). ENSO feedbacks and their relationships with the mean state in a flux adjusted ensemble. *Climate Dynamics*, *52*(12), 7189–7208. https://doi.org/10.1007/s00382-016-3270-9

Ferster, B. S., Fedorov, A. V., Guilyardi, E., & Mignot, J. (2023). The effect of Indian Ocean temperature on the Pacific trade winds and enso. *Geophysical Research Letters*, *50*(20), e2023GL103230. https://doi.org/10.1029/2023GL103230

Fredriksen, H.-B., Berner, J., Subramanian, A. C., & Capotondi, A. (2020). How does El Niño-Southern oscillation change under global warming–A first look at CMIP6. *Geophysical Research Letters*, *47*(22), e2020GL090640. https://doi.org/10.1029/2020GL090640

Fu, M., & Fedorov, A. (2023). The role of bjerknes and shortwave feedbacks in the tropical Pacific SST response to global warming. *Geophysical Research Letters*, *50*(19), e2023GL105061. https://doi.org/10.1029/2023GL105061

Furtado, J. C., Di Lorenzo, E., Anderson, B. T., Schneider, N., Bond, N. A., & Bracco, A. (2012). Linkages between the north Pacific oscillation and central tropical Pacific SSTS at low frequencies. *Climate Dynamics*, *39*(12), 2833–2846. https://doi.org/10.1007/s00382-011-1245-4

Gan, R., Liu, Q., Huang, G., Hu, K., & Li, X. (2023). Greenhouse warming and internal variability increase extreme and central Pacific el niño frequency since 1980. *Nature Communications*, *14*(1), 394. https://doi.org/10.1038/s41467-023-36053-7

Geng, T., Cai, W., Jia, F., & Wu, L. (2024). Decreased enso post-2100 in response to formation of a permanent El Niño-like state under greenhouse warming. *Nature Communications*, *15*(1), 5810. https://doi.org/10.1038/s41467-024-50156-9

Geng, T., Cai, W., Wu, L., Santoso, A., Wang, G., Jing, Z., et al. (2022). Emergence of changing central-pacific and eastern-pacific El Niño-Southern oscillation in a warming climate. *Nature Communications*, *13*(1), 6616. https://doi.org/10.1038/s41467-022-33930-5

Haszpra, T., Herein, M., & Bódai, T. (2020). Investigating enso and its teleconnections under climate change in an ensemble view – A new perspective. *Earth System Dynamics*, *11*(1), 267–280. https://doi.org/10.5194/esd-11-267-2020

Hawkins, E., & Sutton, R. (2009). The potential to narrow uncertainty in regional climate predictions. *Bulletin of the American Meteorological Society*, *90*(8), 1095–1108. https://doi.org/10.1175/2009BAMS2607.1

Heede, U., & Fedorov, A. (2021). Eastern equatorial Pacific warming delayed by aerosols and thermostat response to CO_2 increase. *Nature Climate Change*, *11*(8), 696–703. https://doi.org/10.1038/s41558-021-01101-x

Heede, U., & Fedorov, A. (2023a). Towards understanding the robust strengthening of ENSO and more frequent extreme El Niño events in CMIP6 global warming simulations. *Climate Dynamics*, *61*, 3047–3060. https://doi.org/10.1007/s00382-023-06856-x

Heede, U., & Fedorov, A. (2023b). Colder eastern equatorial Pacific and stronger walker circulation in the early 21st century: Separating the forced response to global warming from natural variability. *Geophysical Research Letters*, *50*(3), e2022GL101020. https://doi.org/10.1029/2022GL101020

Hou, M., & Tang, Y. (2022). Recent progress in simulating two types of enso - From cmip5 to cmip6. *Frontiers in Marine Science*, *9*, 986780. https://doi.org/10.3389/fmars.2022.986780

Hu, A., Richter, I., Okumura, Y., Burls, N., Keenlyside, N., Parfitt, R., et al. (2025). Unraveling the complexity of global climate dynamics: Interactions among el niño-southern oscillation, Atlantic meridional overturning circulation, and tropical basins across different timescales. *Ocean-Land-Atmosphere Research*, *4*, 0096. https://doi.org/10.34133/olar.0096

Hu, S., & Fedorov, A. V. (2017). The extreme el niño of 2015-2016 and the end of global warming hiatus. *Geophysical Research Letters*, *44*(8), 3816–3824. https://doi.org/10.1002/2017GL072908

IPCC. (2021). In V. Masson-Delmotte, P. Zhai, A. Pirani, S. L. Connors, C. Péan, S. Berger, et al. (Eds.), *Climate change 2021: The physical science basis. Contribution of working group I to the sixth assessment report of the intergovernmental panel on climate change*. Cambridge University Press. https://doi.org/10.1017/9781009157896

Kao, H.-Y., & Yu, J.-Y. (2009). Contrasting eastern-pacific and central-pacific types of enso. *Journal of Climate*, *22*(3), 615–632. https://doi.org/10.1175/2008JCLI2309.1

Kelley, M., Schmidt, G. A., Nazarenko, L. S., Bauer, S. E., Ruedy, R., Russell, G. L., et al. (2020). GISS-E2.1: Configurations and climatology. *Journal of Advances in Modeling Earth Systems*, *12*(8), e2019MS002025. https://doi.org/10.1029/2019ms002025

Kohyama, T., Hartmann, D. L., & Battisti, D. S. (2018). Weakening of nonlinear ENSO under global warming. *Geophysical Research Letters*, *45*(16), 8557–8567. https://doi.org/10.1029/2018GL079085

Lee, J., Planton, Y. Y., Gleckler, P. J., Sperber, K. R., Guilyardi, E., Wittenberg, A. T., et al. (2021). Robust evaluation of ENSO in climate models: How many ensemble members are needed? *Geophysical Research Letters*, *48*(20), e2021GL095041. https://doi.org/10.1029/2021GL095041

Lehner, F., Deser, C., Maher, N., Marotzke, J., Fischer, E. M., Brunner, L., et al. (2020). Partitioning climate projection uncertainty with multiple large ensembles and cmip5/6. *Earth System Dynamics*, *11*(2), 491–508. https://doi.org/10.5194/esd-11-491-2020

Li, J., Xie, S.-P., Cook, E., Morales, M. S., Christie, D. A., Johnson, N. C., et al. (2013). El niño modulations over the past seven centuries. *Nature Climate Change*, *3*(9), 822–826. https://doi.org/10.1038/nclimate1936

Maher, N., Matei, D., Milinski, S., & Marotzke, J. (2018). Enso change in climate projections: Forced response or internal variability? *Geophysical Research Letters*, *45*(20), 11390–11398. https://doi.org/10.1029/2018GL079764

Maher, N., Milinski, S., & Ludwig, R. (2021). Large ensemble climate model simulations: Introduction, overview, and future prospects for utilising multiple types of large ensemble. *Earth System Dynamics*, *12*(2), 401–418. https://doi.org/10.5194/esd-12-401-2021

Maher, N., Tabarin, T. P., & Milinski, S. (2022). Combining machine learning and smiles to classify, better understand, and project changes in enso events. *Earth System Dynamics*, *13*(3), 1289–1304. https://doi.org/10.5194/esd-13-1289-2022

Maher, N., Wills, R. C. J., DiNezio, P., Klavans, J., Milinski, S., Sanchez, S. C., et al. (2023). The future of the el niño-southern oscillation: Using large ensembles to illuminate time-varying responses and inter-model differences. *Earth System Dynamics*, *14*(2), 413–431. https://doi.org/10.5194/esd-14-413-2023

Möller, V., van Diemen, R., Matthews, J., Méndez, C., Semenov, S., Fuglestvedt, J., & Reisinger, A. (2022). Annex II: Glossary. In H.-O. Pörtner, et al. (Eds.), *Climate change 2022: Impacts, adaptation and vulnerability. Contribution of working group ii to the sixth assessment report of the intergovernmental panel on climate change* (pp. 2897–2930). Cambridge University Press. https://doi.org/10.1017/9781009325844.029

O'Brien, J. P., & Deser, C. (2023). Quantifying and understanding forced changes to unforced modes of atmospheric circulation variability over the north Pacific in a coupled model large ensemble. *Journal of Climate*, *36*(1), 19–37. https://doi.org/10.1175/JCLI-D-22-0101.1

Olonscheck, D., Suarez-Gutierrez, L., Milinski, S., Beobide-Arsuaga, G., Baehr, J., Fröb, F., et al. (2023). The new max Planck institute grand ensemble with CMIP6 forcing and high-frequency model output. *Journal of Advances in Modeling Earth Systems*, *15*(10), e2023MS003790. https://doi.org/10.1029/2023MS003790

Parker, D. E., Wilson, H., Jones, P. D., Christy, J. R., & Folland, C. K. (1996). The impact of Mount Pinatubo on world-wide temperatures. *International Journal of Climatology*, *16*(5), 487–497. https://doi.org/10.1002/(SICI)1097-0088(199605)16:5⟨487::AID-JOC39⟩3.0.CO;2-J

Pizarro, O., Shaffer, G., Dewitte, B., & Ramos, M. (2002). Dynamics of seasonal and interannual variability of the Peru-Chile undercurrent. *Geophysical Research Letters*, *29*(12). https://doi.org/10.1029/2002GL014790

Planton, Y. Y., Guilyardi, E., Wittenberg, A. T., Lee, J., Gleckler, P. J., Bayr, T., et al. (2021). Evaluating climate models with the clivar 2020 ENSO metrics package. *Bulletin of the American Meteorological Society*, *102*(2), E193–E217. https://doi.org/10.1175/BAMS-D-19-0337.1

Planton, Y. Y., Lee, J., Wittenberg, A. T., Gleckler, P. J., Guilyardi, Ã., McGregor, S., & McPhaden, M. J. (2024). Estimating uncertainty in simulated ENSO statistics. *Journal of Advances in Modeling Earth Systems*, *16*(9), e2023MS004147. https://doi.org/10.1029/2023MS004147

Pontes, G. M., da Silva Dias, P. L., & Menviel, L. (2025). Rapid communication: Nonlinear sensitivity of the el Niño–southern oscillation across climate states. *Climate of the Past*, *21*(6), 1079–1091. https://doi.org/10.5194/cp-21-1079-2025

Rodgers, K. B., Lee, S.-S., Rosenbloom, N., Timmermann, A., Danabasoglu, G., Deser, C., et al. (2021). Ubiquity of human-induced changes in climate variability. *Earth System Dynamics*, *12*(4), 1393–1411. https://doi.org/10.5194/esd-12-1393-2021

Stuivenvolt-Allen, J., Fedorov, A. V., Fu, M., & Heede, U. (2025). Widening of wind stress anomalies amplifies ENSO in a warming climate. *Journal of Climate*, *38*(2), 497–512. https://doi.org/10.1175/JCLI-D-24-0126.1

Swart, N. C., Cole, J. N. S., Kharin, V. V., Lazare, M., Scinocca, J. F., Gillett, N. P., et al. (2019). The Canadian Earth system model version 5 (CanESM5.0.3). *Geoscientific Model Development*, *12*(11), 4823–4873. https://doi.org/10.5194/gmd-12-4823-2019

Takahashi, K., Montecinos, A., Goubanova, K., & Dewitte, B. (2011). ENSO regimes: Reinterpreting the canonical and Modoki El Niño. *Geophysical Research Letters*, *38*(10), L10704. https://doi.org/10.1029/2011GL047364

Tatebe, H., Ogura, T., Nitta, T., Komuro, Y., Ogochi, K., Takemura, T., et al. (2019). Description and basic evaluation of simulated mean state, internal variability, and climate sensitivity in MIROC6. *Geoscientific Model Development*, *12*(7), 2727–2765. https://doi.org/10.5194/gmd-12-2727-2019

Ting, M., Kushnir, Y., Seager, R., & Li, C. (2009). Forced and internal twentieth-century sst trends in the north Atlantic. *Journal of Climate*, *22*(6), 1469–1481. https://doi.org/10.1175/2008JCLI2561.1

Trenberth, K. E. (1997). The definition of El niño. *Bulletin of the American Meteorological Society*, *78*, 2771–2778. https://doi.org/10.1175/1520-0477(1997)078⟨2771:TDOENO⟩2.0.CO;2

Vaittinada Ayar, P., Battisti, D. S., Li, C., King, M., Vrac, M., & Tjiputra, J. (2023). A regime view of ENSO flavors through clustering in CMIP6 models. *Earth's Future*, *11*, e2022EF003460. https://doi.org/10.1029/2022EF003460

Wang, H.-J., Zhang, R.-H., Cole, J., & Chavez, F. (1999). El Niño and the related phenomenon southern oscillation (ENSO): The largest signal in interannual climate variation. *Proceedings of the National Academy of Sciences*, *96*(20), 11071–11072. https://doi.org/10.1073/pnas.96.20.11071

Wengel, C., Lee, S., Stuecker, M., Timmermann, A., Chu, J. E., & Schloesser, F. (2021). Future high-resolution El Niño/Southern oscillation dynamics. *Nature Climate Change*, *11*(9), 758–765. https://doi.org/10.1038/s41558-021-01132-4

Wills, R. C. J., Dong, Y., Proistosecu, C., Armour, K. C., & Battisti, D. S. (2022). Systematic climate model biases in the large-scale patterns of recent sea-surface temperature and sea-level pressure change. *Geophysical Research Letters*, *49*(17), e2022GL100011. https://doi.org/10.1029/2022GL100011

Ziehn, T., Chamberlain, M. A., Law, R. M., Lenton, A., Bodman, R. W., Dix, M., et al. (2020). The Australian Earth system model: Access-esm1.5. *Journal of Southern Hemisphere Earth Systems Science*, *70*(1), 193–214. https://doi.org/10.1071/ES19035